Available online at www.sciencedirect.com
ScienceDirect
Ocean Modelling 22 (2008) 12–25
Ocean Modelling
www.elsevier.com/locate/ocemod

Obstruction grids for spectral wave models ☆

Arun Chawla *,[1], Hendrik L. Tolman [2]

Marine Modeling and Analysis Branch, 5200 Auth Road, Room 209, Camp Springs, MD 20746, USA

Received 15 June 2007; received in revised form 31 December 2007; accepted 7 January 2008
Available online 10 February 2008

Abstract

An algorithm has been developed to construct obstruction grids for spectral wave models to properly account for wave attenuation by unresolved islands. The algorithm uses the GSHHS coastline dataset, and accounts for islands overlapping grid cells as well as the orientation of islands in neighboring cells. The algorithm has been validated by conducting numerical experiments with the wave model WAVEWATCH III. The numerical experiments consisted of a swell propagating through French Polynesia with grids of various spatial resolutions (2′, 4′, 8′, 15′ and 30′). The systematic patterns of energy attenuation behind the islands in the highest resolution grid, with a limited number of unresolved islands represented by obstructions, were well reproduced by the lower resolution grids where most islands are represented by obstruction grids. The algorithm is part of a larger software package that has been developed to build grids for spectral wave models, in particular WAVEWATCH III.

Keywords: WAVEWATCH III; GSHHS; Sub-grid obstructions; Swell propagation; Garden Sprinkler Effect

1. Introduction

Blocking of ocean waves by islands and barrier reefs that are too small to be resolved by a numerical grid can be a significant source of error in wave prediction models. To explicitly account for the wave height attenuation due to these features requires grids with excessively high resolution which become economically unfeasible for practical calculations. Alternatively, such features can be modeled as sub-grid obstructions where the energy flux is attenuated using obstruction grids (Hardy and Young, 1996; Hardy et al., 2001; Holthuijsen et al., 2001; Tolman, 2003). The concept works well and Tolman (2003) showed that using obstruction grids significantly reduces the bias between ERS-2 altimeter data and numerical model results. However, the obstruction grids used in the study had to be developed manually. In this paper we present an algorithm for automatically developing obstruction grids that can then be used with sub-grid modeling algorithms. As will be demonstrated in Section 2, this requires coastline information rather than bathymetric data. Furthermore, in recently developed "multi-grid" wave models (Tolman, 2006) consistent obstructions for several grids at different resolutions are needed. An automated approach to generating obstructions is expected to be conducive to provide consistency between grids.

The obstruction grid algorithm has been developed to be used with the method of accounting for obstructions as outlined in Tolman (2003) and implemented in the spectral ocean wave model WAVEWATCH III (Tolman, 2002b, 2006). It builds the corresponding obstructions for a given grid using a global shoreline database. Since the concept of using sub-grid algorithms has already been tested with altimeter data in a full wave model application (Tolman, 2003), the tests in this paper are limited to study how well the obstruction effects are reproduced using the obstruction grids developed here. This is done by conducting a swell propagation experiment with WAVEWATCH III (henceforth referred to as **WW3**) through a region consisting of

☆ MMAB contribution No. 255.

* Corresponding author. Tel.: +1 301 763 8000x7209; fax: +1 301 763 8545.
E-mail addresses: arun.chawla@noaa.gov (A. Chawla), hendrik.tolman@noaa.gov (H.L. Tolman).
[1] SAIC-GSO at NOAA/NCEP/EMC.
[2] GSO at NOAA/NCEP/EMC.

1463-5003/$ - see front matter © 2008 Elsevier Ltd. All rights reserved.
doi:10.1016/j.ocemod.2008.01.003

a large number of islands (atolls) using grids with different resolutions. The wave height patterns in the high resolution grids (where most islands are well resolved) and the low resolution grids (where the islands are represented by obstructions) are compared to assess how well the obstructions reproduce the wave height attenuation due to the islands. Although the algorithm has been developed for **WW3** it can be used with any model that uses similar obstruction grids to account for sub-grid attenuation.

The approach used here considers obstructions along the x and y directions. This differs from the approach used by Hardy et al. (2001) where the obstructions are determined as a function of wave direction. Both methods perform well as is shown in their respective publications. A detailed comparison of the two methodologies is beyond the scope of this study. Note furthermore that obstructions are only a proxy for modeling islands that are not well resolved. Because the obstruction grid does not identify where in a grid cell the obstruction occurs, accurate model results can not be expected in an area of a few grid increments around such islands. Instead, obstructions are intended to describe effects of island blocking on larger scales. Accurate solutions close to islands with significant wave blocking are only to be expected if such islands are properly resolved in a model.

2. GSHHS database

The obstruction grid algorithm uses the GSHHS (global self-consistent hierarchical high resolution shoreline) database developed by Wessel and Smith (1996) to generate the data. This database includes five different types of boundaries – coastal boundaries, lakes, islands in lakes and ponds in islands in lakes. The boundary data are stored as polygons. Each polygon consists of a number of discrete points and represents a closed boundary.

There are several reasons for using this database. First, it is a comprehensive and accurate record of global shorelines. In full resolution there are 188,606 polygons in the database of which 180,509 are coastal boundaries. Out of these, 180,466 boundaries enclose an area less than 12,400 km^2, corresponding to a grid square of $1^\circ \times 1^\circ$ at the equator. Fig. 1 shows the cumulative distribution of these boundaries as a function of the area they enclose (in km^2). Most of these boundaries (over 99% of them) have an area less than 6 km^2. In comparison, a grid cell in a high resolution $2'$ grid (e.g. NGDC, 2006) covers approximately 14 km^2. Thus, a large majority of the boundaries in GSHHS cannot be resolved even in high resolution global bathymetry data sets. Second, identifying the shorelines as closed polygons accurately represents features such as atolls which by themselves cover very little area but act as effective barriers to wave propagation (see Fig. 1 in Tolman, 2003). Using polygons also makes it trivial to determine the proportion of any grid cell being blocked. Finally, using polygons to develop obstruction grids makes it convenient to generate additional polygons for boundaries that are not represented in the global data sets (e.g. local dikes, breakwaters, etc.). Note that the GSHHS database used here can easily be extended to include other small scale structures (cf. Holthuijsen et al., 2001), reefs that effectively block swell propagation (cf. Hardy et al., 2001) or areas to be taken from a model domain that are considered irrelevant for a study.

3. Sub-grid obstruction algorithm

The obstruction algorithm introduced by Tolman (2003) requires obstruction grids for both grid axes of the spatial

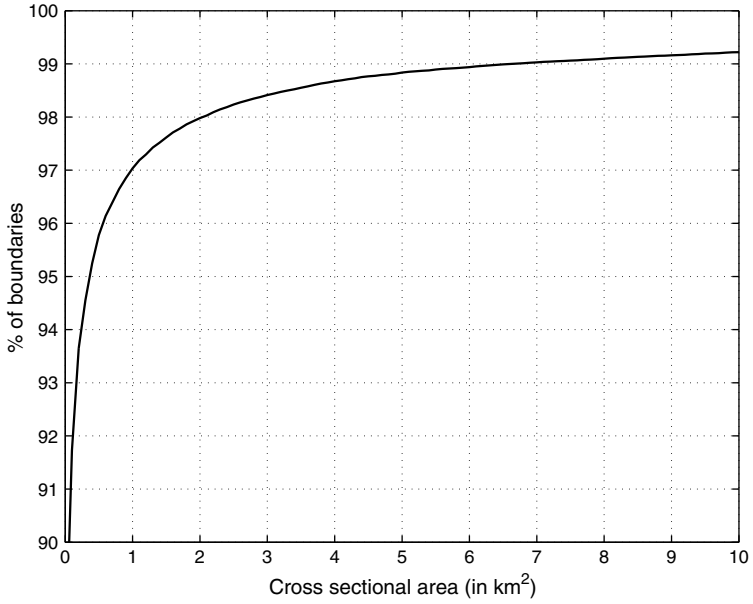

Fig. 1. Cumulative distribution of coastal boundaries with area less than 12,400 km^2 (number of boundaries = 180,446).

grid. The main elements of the method are reproduced here and the reader is referred to the original paper (Tolman, 2003) for a detailed discussion. The methodology accounts for the effects of unresolved islands by suppressing the energy flux across discrete grid cell boundaries. The modified numerical equation for spatial propagation (here limited to 1D for simplicity) is given by

$$F_i^{n+1} = F_i^n + \frac{\Delta t}{\Delta x}[\alpha_{i,-} G_{i,-} - \alpha_{i,+} G_{i,+}] \tag{1}$$

where n and i correspond to time and space counters, Δt and Δx are the corresponding time and space step, respectively, F_i is the spectral action density, $G_{i,-}$ is the energy flux across the common cell boundary between grid points i and $i-1$, $G_{i,+}$ is the energy flux across the common cell boundary between grid points i and $i+1$, and $\alpha_{i,-}$ and $\alpha_{i,+}$ are the transparencies at the corresponding cell boundaries. The value of the transparency ranges from 0 (full obstruction) to 1 (no obstruction). The transparencies in WAVEWATCH III can either be defined at the cell boundaries, leading to a staggered grid, or at the cell centers. When the transparency is defined at the cell center (given by α_i) they are converted to transparencies at cell boundaries inside the model. Detailed information relating the cell center transparencies to the cell boundary transparencies can be found in Tolman (2003). The algorithm developed in this paper to generate the data assumes that the transparencies are defined at the cell centers though it can be adapted for cell boundaries as well.

In WAVEWATCH III the transparency data are provided as obstruction grids for the x and y directions. The obstruction S represents the fraction of energy being blocked in the cell and is related to the transparency α by

$$S = 1 - \alpha \tag{2}$$

Fig. 2a shows an obstruction in a single cell. The obstructions for this cell in the x and y direction (hereafter referred to as ***Sx*** and ***Sy***, respectively) are given by

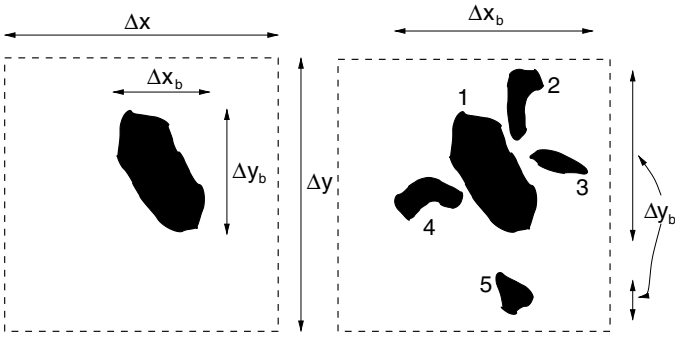

(a) Single obstruction (b) Multiple obstructions

Fig. 2. Obstructions in a single cell: (a) single obstruction; (b) multiple obstructions.

$$\boldsymbol{Sx} = \frac{\Delta y_b}{\Delta y}; \quad \boldsymbol{Sy} = \frac{\Delta x_b}{\Delta x} \tag{3}$$

where, Δx_b, Δy_b, Δx and Δy represent the length of the obstructions and the cell dimensions in x and y direction, respectively. Obstruction grid values for dry (land) cells are kept at 0 and non-zero values are only generated for wet cells with unresolved boundaries in them. To prevent spurious attenuation of swell traveling into the coast, obstruction values of cells next to dry cells are also set to 0. For multiple boundaries, only that part of a boundary is considered which plays a role in the obstruction of wave energy. Fig. 2b shows how the boundary segments are computed. Although obstructions account for the fraction of energy being blocked in a cell, they do not account for where in the cell the blocking occurs. This has some implications in the development of the obstruction grids.

When boundaries overlap cells there are potential problems in determining obstruction data as was identified in Fig. 1 of Tolman (2003) and as is shown in Fig. 3a. In the figure two boundaries cover multiple cells. Boundary 1 overlaps cells **B**, **C** and **F**, while boundary 2 overlaps cells **E** and **H**. Boundary 1 blocks wave energy propagation in the x direction from cell **A** to cell **C** completely. However,

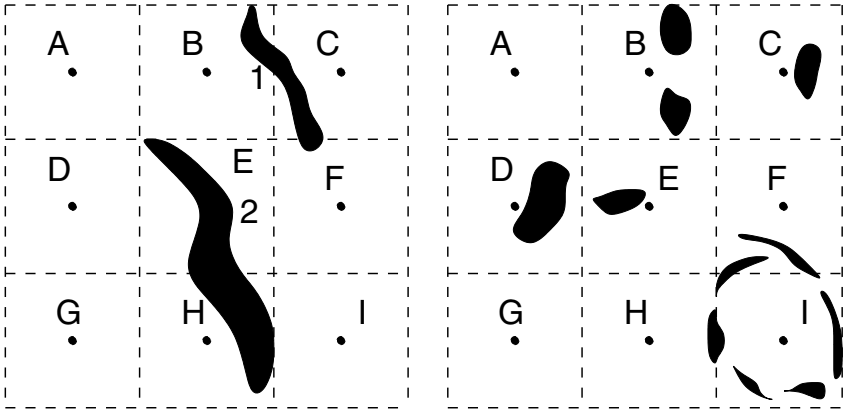

(a) Obstructions overlapping cells (b) Impact of neighboring cells

Fig. 3. Obstructions in multiple cell: (a) obstructions overlapping cells; (b) impact of neighboring cells.

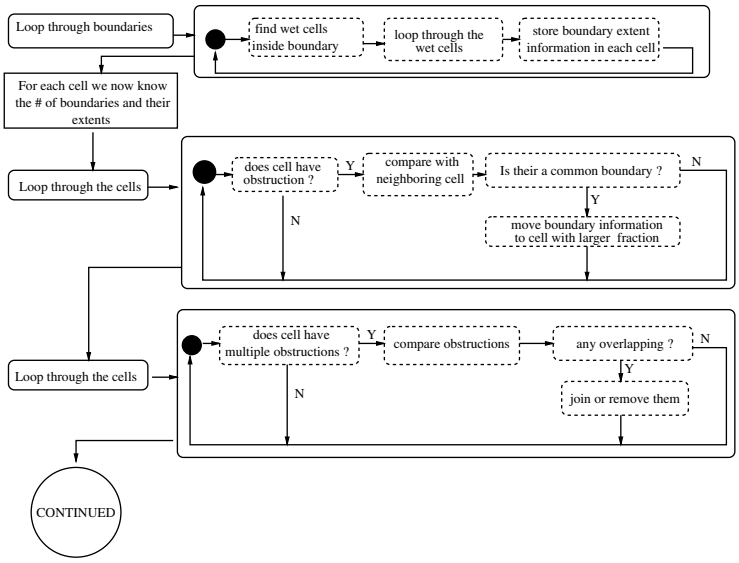

(a) Part I

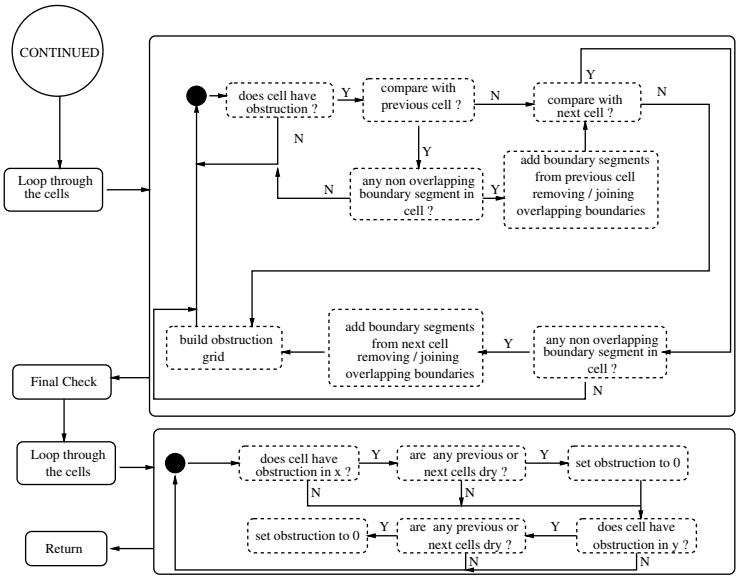

(b) Part II

Fig. 4. Flow chart of the obstruction algorithm: (a) Part I; (b) Part II.

if ***Sx*** values for cell **B** and cell **C** are to be determined based only on the proportion of the boundary found inside each cell, then only partial blocking in each cell will take place. Alternatively, since the same boundary segment occurs in both the cells, we could move the segment from one cell to the other and use the combined segment to compute the obstruction grids. Naturally, the smaller segment is moved to the cell with the larger segment. This will lead to complete blocking in one grid and no blocking in the other. Since our aim is to model the correct amount of sub-grid energy at the resolution of the coarse grid, moving the segment from one cell to the other is acceptable. The argument does not extend to ***Sx*** computations in cell **F** as the obstruction there occurs at a different row, and is not affected by the obstructions in cells **B** and **C** (at least at the local level). The same argument also holds for ***Sy*** computations in cells **E** and **H** with respect to boundary 2. Note that moving of segments is done for each direction individually; for ***Sy*** the two segments in **B** and **C** are left in their original cells, but the segment from **F** will now be moved to **C**.[3]

A final factor to consider in building the obstruction grids are the orientations of the boundaries in neighboring cells. Since obstruction grids only compute the attenuation of energy due to sub-grid blocking, and not where in the

[3] Moving obstructions to a single cell also avoids "double counting" as identified in Fig. 1 of Tolman (2003).

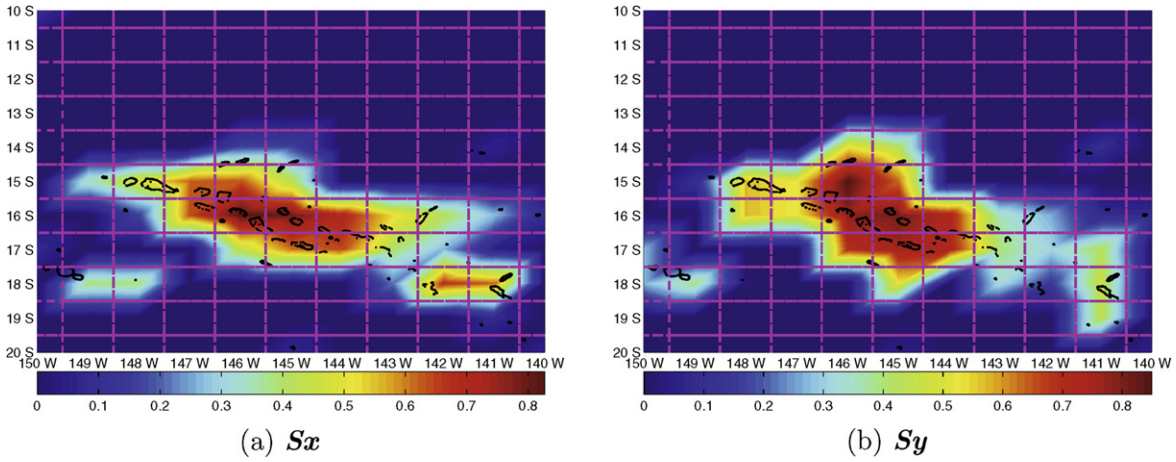

Fig. 5. Obstructions for a 1° resolution grid of the Tuamotu archipelago in French Polynesia. Black lines represent the GSHHS polygons and magenta lines represent individual cell boundaries. Obstructions are generated taking into account neighboring cell information on both sides: (a) ***Sx***; (b) ***Sy***.

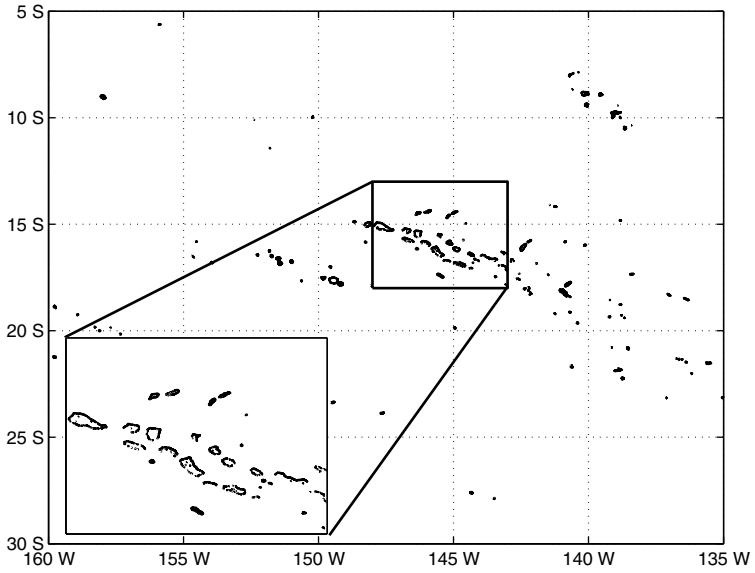

Fig. 6. French Polynesian islands. The grid domain includes the archipelagos of Marquesas (5–10°S and 143–137°W), Tuamotu (15–20°S and 149–140°W) and the Society islands (15–18°S and 153–149°W). Inset figure shows a closer look of the Tuamotu atolls.

cell this blocking occurs, the orientation of boundaries in neighboring cells can have a significant impact on the obstruction. This is illustrated in Fig. 3b. In cell **B** the blocking occurs on the top and bottom part of the cell, while in cell **C** the blocking occurs in the middle part of the cell. As a result, swell propagation in the x direction would be completely blocked. However, the obstructions for the individual cells are approximately 0.5, and would lead to spurious swell penetration. Alternatively, the island in cell **E** lies in the shadow zone of the island in cell **D** and should not play a role in the overall obstruction process. However, if only obstructions of individual cells are considered, this scenario would lead to spurious swell suppression. We can take these effects into account by including the boundary segments of the neighboring cells when building the obstruction grids.

If obstruction grids are taking obstructions in neighboring cells into account, the question arises how many neighboring cells should be taken into account. Because we are trying to simulate local processes, at the scale of a grid cell, it appears appropriate to consider only direct neighboring cells within this approach. Using the schematic in Fig. 3b we look at the impact of neighboring cells on ***Sx*** values.

Table 1
The different obstruction scenarios used in the numerical experiment

Test	Obstruction grid
NO-OB	No obstruction accounted for
OB-0	Obstruction accounted in individual cell only
OB-1	Obstruction includes up wind neighboring cell information
OB-2	Obstruction includes both up wind and down wind neighboring cell information

First, consider using both neighbors. In this case contributions to ***Sx*** for cell **A** come from cell **B**, for cell **B** from cells **B** and **C**, and for cell **C** also from cell **B**. While this would account for the impact of neighboring cells, we can also identify over-obstruction in several cases. First, cells **A** and **F** contain no obstructions and thus should have $\boldsymbol{Sx} = 0$. However, because information from neighboring cells is used, non-zero values will be registered in these cells. This is easily remedied by ensuring that obstruction values are only assigned if the cell in question contributes to the obstruction of wave energy. Then the ***Sx*** values in cells **A** and **F** (because of no boundaries) as well as cell **E** (because the boundary lies in a shadow zone of neighboring cells) would be set to 0. This however does not completely remove the over obstruction. For energy propagating from left to right, the effects of cells **B** and **C** would be felt both in cell **B** as well as cell **C**.

Alternatively, we can intentionally introduce directional preference in our ***Sx*** computations by taking only neighbors from one side into account. This results in two sets of ***Sx*** grids, one which is built taking account of neighbors on the left and the other taking into account neighbors on the right. In the case of the example looking to the left only, the contribution to cell **B** will come from **B** itself and for cell **C** from **B** and **C**. For waves propagating from left to right this creates an obstruction data set with no over obstruction. If on the other hand we take neighbors on the right hand side to compute the ***Sx*** grid then, contribution to cell **C** would now come from **C** itself and for cell **B** from cells **B** and **C**. Again for waves propagating from right to left this set of obstruction values would not lead to over obstruction. Thus, the advantage of having directionally preferred obstruction values is that over obstruction can be avoided. However, the disadvantage is that there are two sets of ***Sx*** grids and the choice of grid depends upon the direction of wave propagation. Similar arguments would hold for ***Sy*** grids with the neighboring cells being above and below. Finally, let us consider the example of an atoll as shown in cell **I** of Fig. 3b. Some of the boundary segments overlap into cells **H** and **F**. For ***Sx*** calculations, the overlap of the boundary segments in cell **H** need to be taken into account and for ***Sy*** calculations, the overlap of the boundary segments in cell **F** need to be taken into account. However, by including the effects of the neighboring cells, full obstructions (in both directions) would be appropriately registered at this cell.

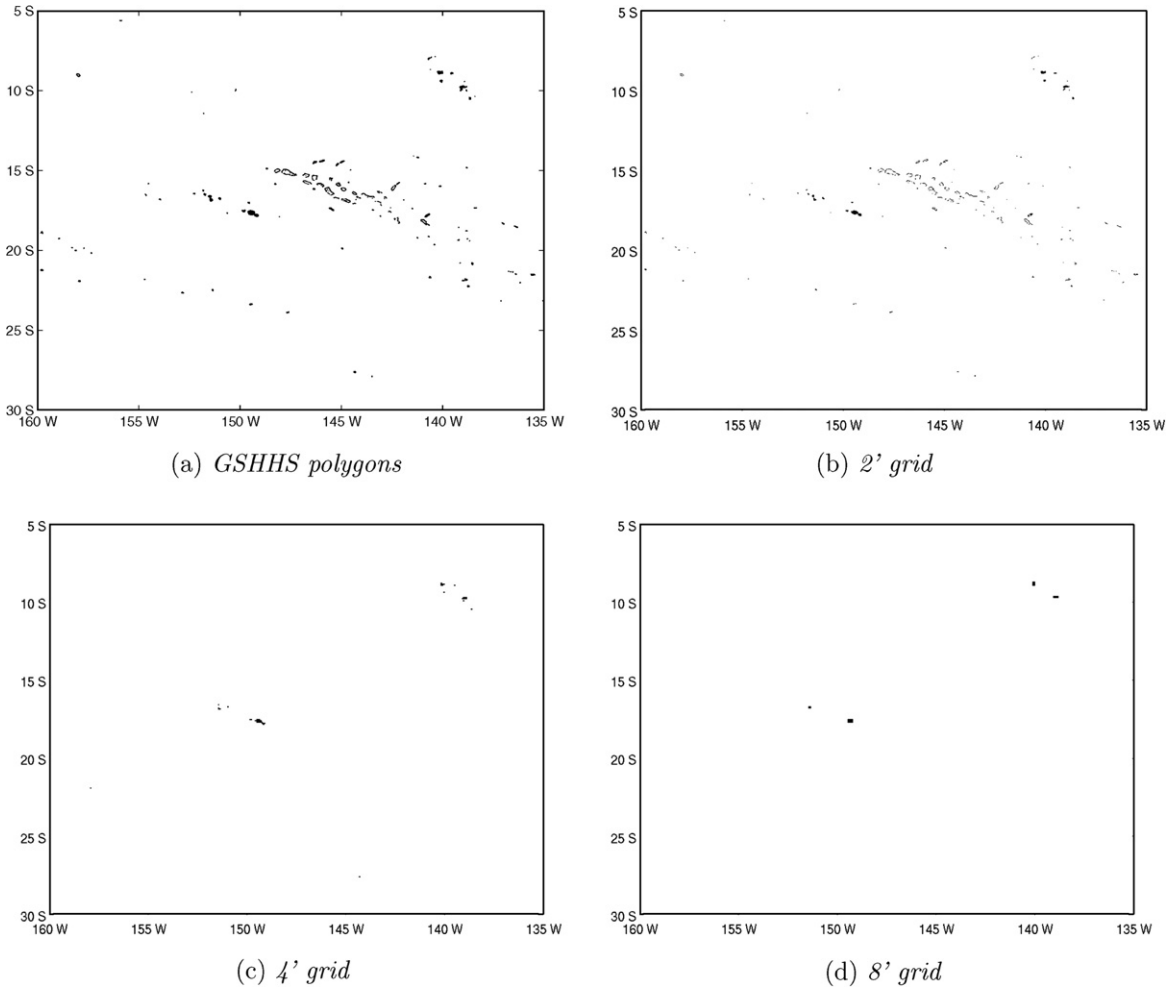

Fig. 7. Land masks for the French Polynesian Islands test case: (a) GSHHS polygons; (b) 2′ grid; (c) 4′ grid; (d) 8′ grid.

A flow chart of the obstruction algorithm that takes into account all the above points is shown in Fig. 4 (split over two figures for clarity). Three separate options have been considered for taking into account neighboring cell information: Option 1, no neighboring cell information is used; Option 2, neighboring cell information from one specified direction is used; Option 3, neighboring cell information from both sides is used. Fig. 5 shows an example of obstructions generated for the Tuamotu archipelago using a 1° resolution grid. The grid resolution is too coarse to resolve the small islands of this archipelago and all energy attenuation has to be accounted for by obstructions. Although individually these islands are very small, together they are very effective in blocking ocean swells as is reflected in the obstruction grids. The accuracy of these obstruction grids is tested in the next section.

4. Numerical tests

To determine how well the obstruction grids attenuate wave energy, a series of swell propagation studies were conducted in three different regions – the Caribbean, Hawaii and French Polynesia. Here we will concentrate only on the French Polynesian islands (Fig. 6) with their numerous atolls and small islands. For a detailed report on the other two test cases see Chawla and Tolman (2007).

Grids with five different spatial resolutions of 2′, 4′, 8′, 15′ and 30′ were constructed. The corresponding global time steps for the grids were 300, 600, 1200, 1800 and 1800 s, respectively. Refraction effects and source terms were switched off in the model runs to eliminate cumulative differences associated with representation of the bathymetry at the different grid resolutions. The aim of this exercise was to see if the energy attenuation in the highest resolution grid is accurately reproduced in the lower resolution grids using obstructions. Effects of obstructed wave energy propagation become evident in spatial distribution of significant wave heights (H_s). When comparing results at two different resolutions, the results were averaged over all the cells in the higher resolution grid that lie inside the cells of the lower resolution grid, so that differences could be assessed directly.

The experiment consists of a constant swell propagating from the North-East at an angle of 45°. The swell is mono-

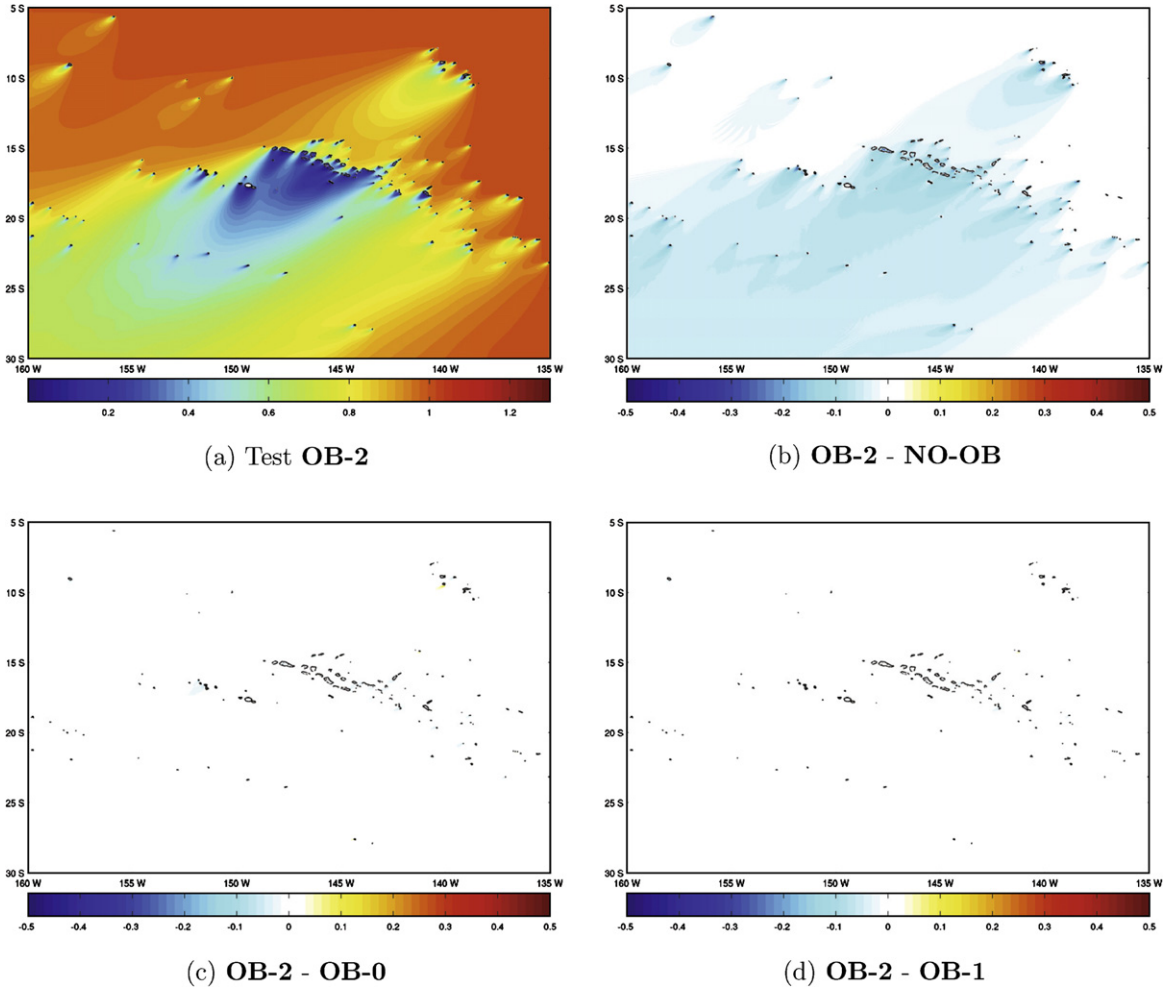

(a) Test **OB-2** (b) **OB-2 - NO-OB**

(c) **OB-2 - OB-0** (d) **OB-2 - OB-1**

Fig. 8. Normalized significant wave heights for 2′ grid. Panel (a) represents the normalized wave height while panels b–d are normalized difference plots: (a) Test **OB-2**; (b) **OB-2**–**NO-OB**; (c) **OB-2**–**OB-0**; (d) **OB-2**–**OB-1**.

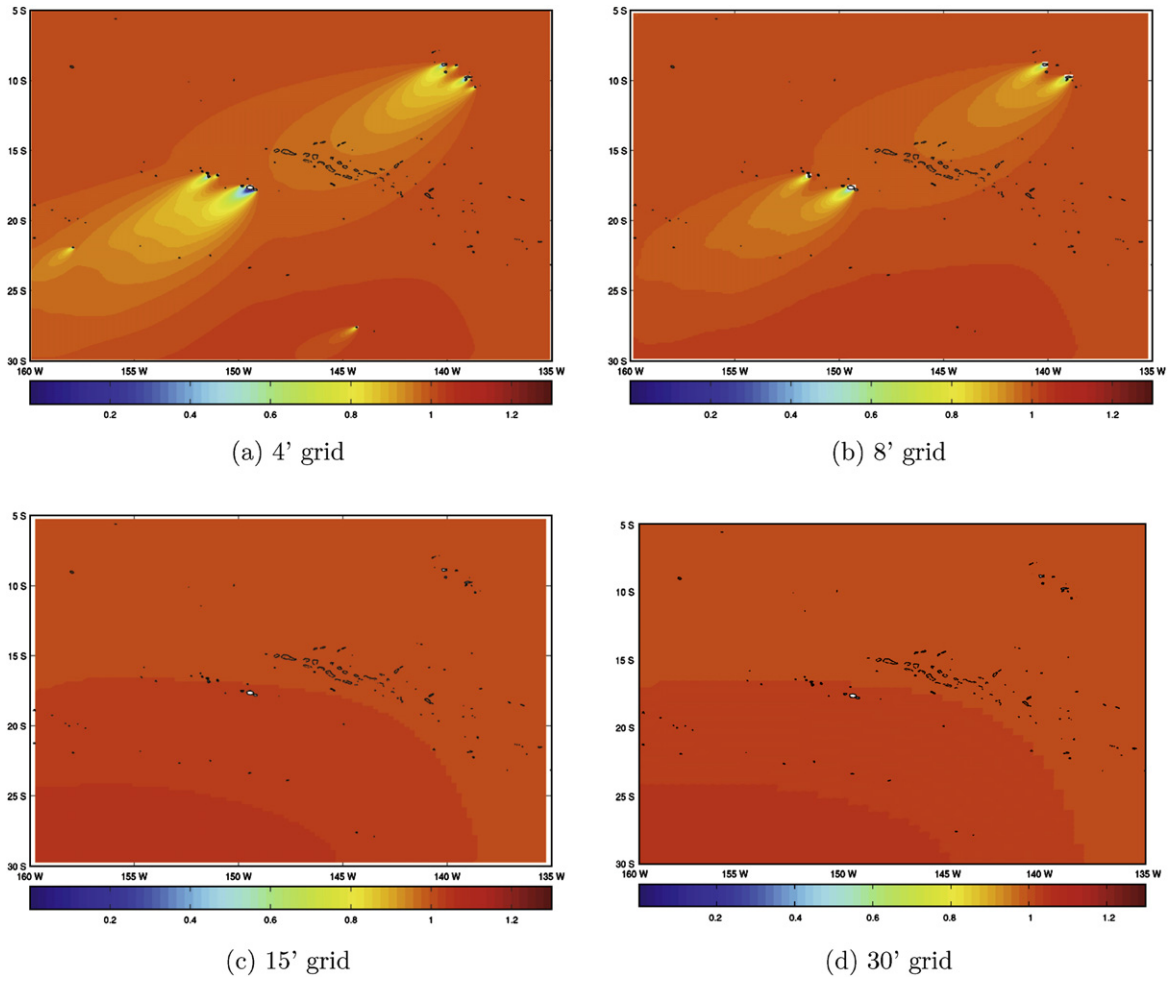

Fig. 9. Normalized significant wave heights for tests without obstructions (**NO-OB**): (a) 4′ grid; (b) 8′ grid; (c) 15′ grid; (d) 30′ grid.

chromatic with a frequency of 0.1 Hz. The directional spreading is given by

$$D(\theta) = \cos^8\left(\frac{(\theta - \theta_p)}{2}\right), \tag{4}$$

where θ_p refers to the peak direction of the swell. The directional spread used here is narrower than usual for wind waves, but broad for ocean swells. Along the Northern and Eastern boundaries the significant wave height (H_{sb}) was set at 4 m. In all the runs the simulations were carried out for 7 days to reach steady state conditions across the region.

When modeling swell propagation with a discrete spectral wave model, spurious disintegration of the wave field may occur. This is known as the "Garden Sprinkler Effect" (GSE) (Booij and Holthuijsen, 1987; Tolman, 2002a). GSE can play a significant role on the wave height patterns behind the islands (see Chawla and Tolman, 2007), and care was taken to apply similar levels of alleviation in all the different resolution runs. An averaging technique from Tolman (2002a) was used to alleviate GSE. Appendix A describes how the parameters for this technique have been determined.

The three different ways to build the obstruction grids have been considered as well as not taking any obstructions into account (see Table 1 for test particulars). Since the swell is propagating from the North-East, the neighbors to the right (up) in x (y) direction are considered when building obstructions for Test **OB-1**.[4]

Fig. 7 shows how well the islands and atolls are resolved in the different grids in comparison to the GSHHS database. Even in the highest resolution grid not all the features observed in the GSHHS database are resolved. As grid resolution decreases a significant number of the islands can no longer be resolved and the model has to rely on obstruction grids to simulate swell attenuation. None of the islands can be resolved in the 15′ and 30′ grids and these grids therefore have not been shown in Fig. 7.

[4] It should be kept in mind that the current version of WAVEWATCH III only allows for one set of obstruction grids in the x and y direction, and if **OB-1** has to be applied as a general technique then the model will have to be modified to read in two obstruction grids for each direction, and the appropriate obstruction used depending on the location of the inflow boundary which is determined by the model for (1). This represents a minor modification to the code.

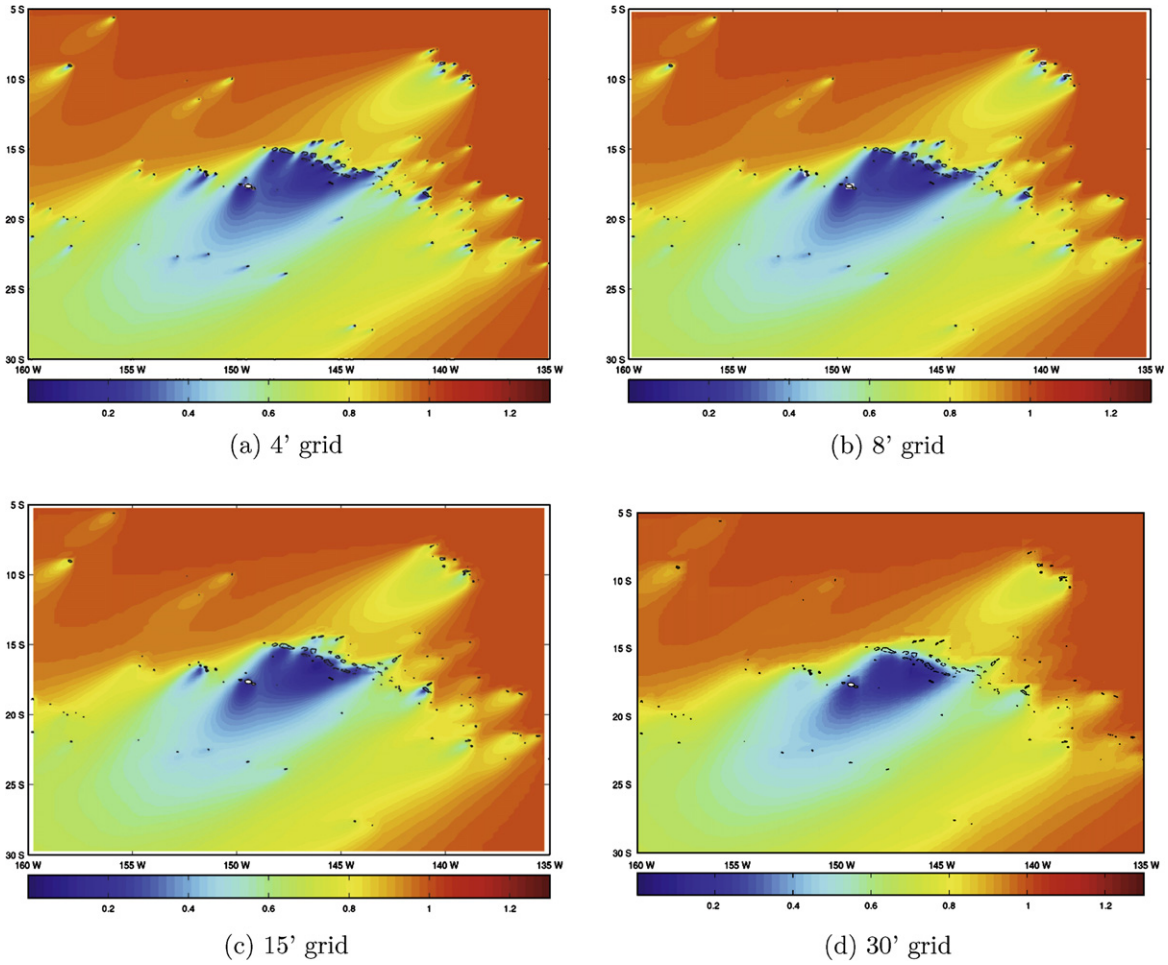

Fig. 10. Normalized significant wave heights for tests with obstructions including both neighboring cells (**OB-2**): (a) 4′ grid; (b) 8′ grid; (c) 15′ grid; (d) 30′ grid.

Before the different scenarios can be compared we need to determine a ground truth solution for our experiment. Fig. 8 shows the significant wave height field for the 2′ grid with obstruction on both sides (Test **OB-2**), and its comparison with the other three scenarios. All wave heights in the plots have been normalized by the incident wave height H_{sb}. As can be seen from the comparisons of Fig. 8b obstruction grids play a significant role in the wave field even at this high resolution. The obstruction grids **OB-0** and **OB-1** yield very similar results to **OB-2** (Fig. 8c and d) showing that at this resolution moving boundary segments that intersect cells works well and including additional information from neighboring cells has no major impact and any of these solutions can be taken as the ground truth. We have chosen the 2′ grid Test **OB-2** as the ground truth (henceforth referred to as **GT**).

The impact of obstructions at the coarser resolutions can be clearly seen in the wave height patterns behind the islands without accounting for obstructions (Fig. 9, **NO-OB**) and with accounting for obstruction (Fig. 10, **OB-2**). We can clearly see that a significant portion of the islands are invisible to the propagating swell at the 4′ and lower resolution grids (Fig. 9). However, including obstruction grids (Fig. 10), qualitatively reproduces the **GT** swell patterns even in the 30′ grid.

To quantify the impact of obstruction grids, difference plots with the **GT** solution for the different scenarios are shown in Figs. 11–14. As expected, not accounting for obstructions (Fig. 11) has an order of magnitude effect on the swell conditions behind the islands with errors larger than 50%. Only accounting for obstructions in the individual cells (Fig. 12) significantly improve the results but there is still some spurious swell penetration behind the islands. Because of the large numbers of small island chains and atolls, accounting for obstruction in the neighboring cells (either on one side or both sides – Figs. 13 and 14, respectively) leads to better estimates of the blocking effect. Accounting for obstructions in neighboring cells on both sides (Fig. 14) overcompensates the energy attenuation in some areas, however overall **OB-1** $\approx$ **OB-2** qualitatively.

The obstruction grid algorithm is part of a software package that has been developed for building grids for **WW3**.[5] The software package includes modules for

[5] Adapting to other spectral wave models should be fairly straightforward.

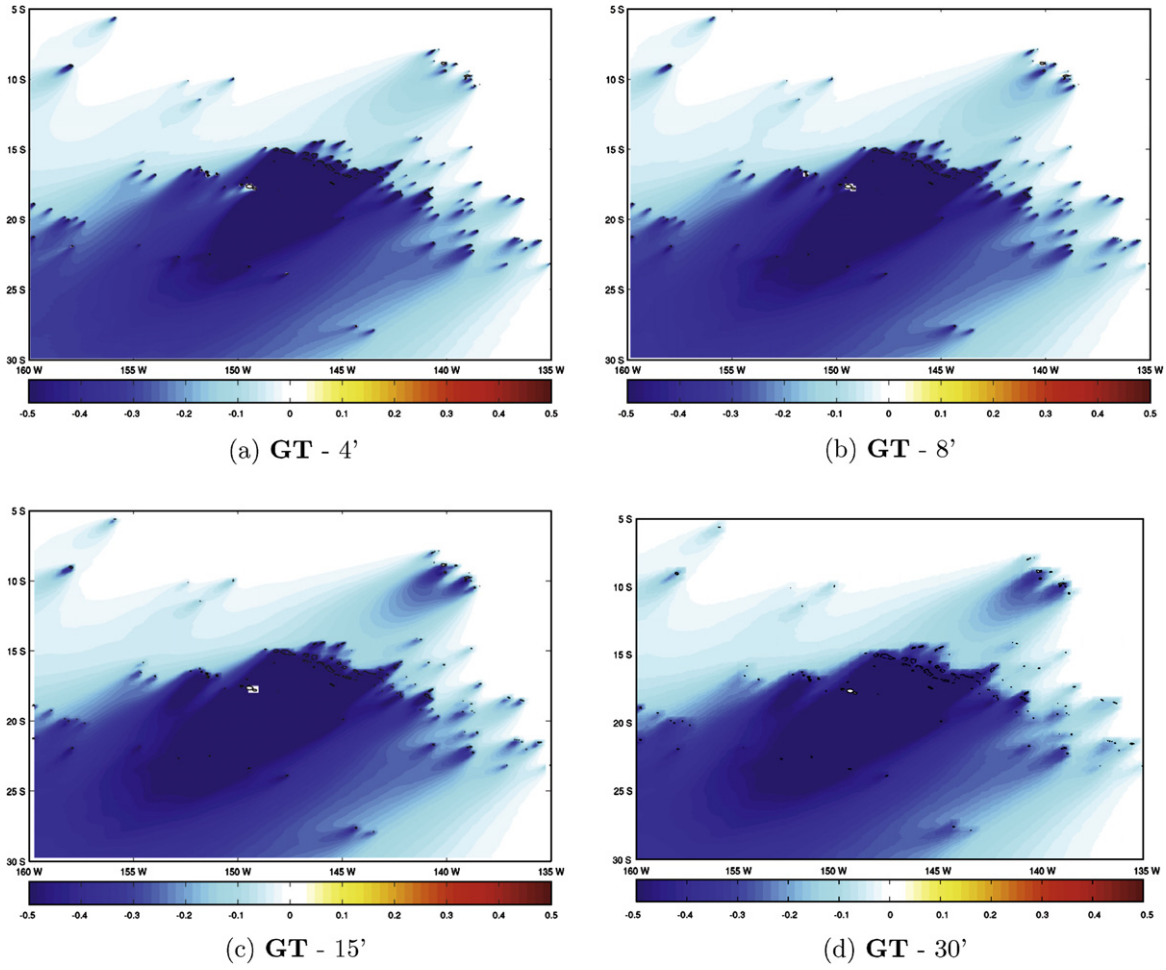

Fig. 11. Normalized difference plots (Ground Truth – Test Case) of wave heights for tests not accounting for obstruction (**NO-OB**): (a) **GT-4′**; (b) **GT-8′**; (c) **GT-15′**; (d) **GT-30′**.

generating bathymetric grids, refining land–sea masks to accurately account for shorelines, cleaning up the grid to remove isolated wet cells, modifying the land–sea mask for active wet cells[6] and developing obstruction grids. The GSHHS coastline database is used for both developing an accurate land–sea mask, and constructing obstruction grids. See Chawla and Tolman (2007) for detailed information on the package.

5. Conclusions

An obstruction grid algorithm has been developed using a global shoreline database (GSHHS) to develop a set of obstruction grids. These data are then used by the WAVEWATCH III model to appropriately scale the energy flux in the spatial propagation numerical scheme and hence simulate the swell blocking effects of unresolved islands. For any given grid cell there are two obstruction values (for the two grid axes) ranging from 0 (no obstruction) to 1 (complete obstruction). The obstruction in any particular direction is determined by the proportion of the cell blocked by islands in that direction. When building the obstructions, the algorithm has the option to not only consider the orientation of islands in the corresponding cell but also the islands in neighboring cells. This significantly improves swell blocking of islands in our test cases. Note that though the GSHHS database has been used here, the algorithm can be used with any polygon based coastline database.

The accuracy of the data generated by the obstruction grid algorithm has been numerically tested in the archipelagos of French Polynesia, Hawaii and the Caribbean region (see Chawla and Tolman, 2007 for the latter two test cases). In all the test cases the waves were propagated diagonally across the grid to show that wave blocking is well simulated even when waves are not aligned with the axes on which the obstructions have been defined. For the archipelagos of French Polynesia tests were also conducted for waves propagating from the East and South-East (figures not shown). In all the different cases, using the obstruction grids the model was able to reproduce swell patterns to within $\pm 10\%$ of the Ground Truth solution. It should be emphasized that the sub-grid

[6] This is specific to multi-grid version of **WW3** Tolman (2006).

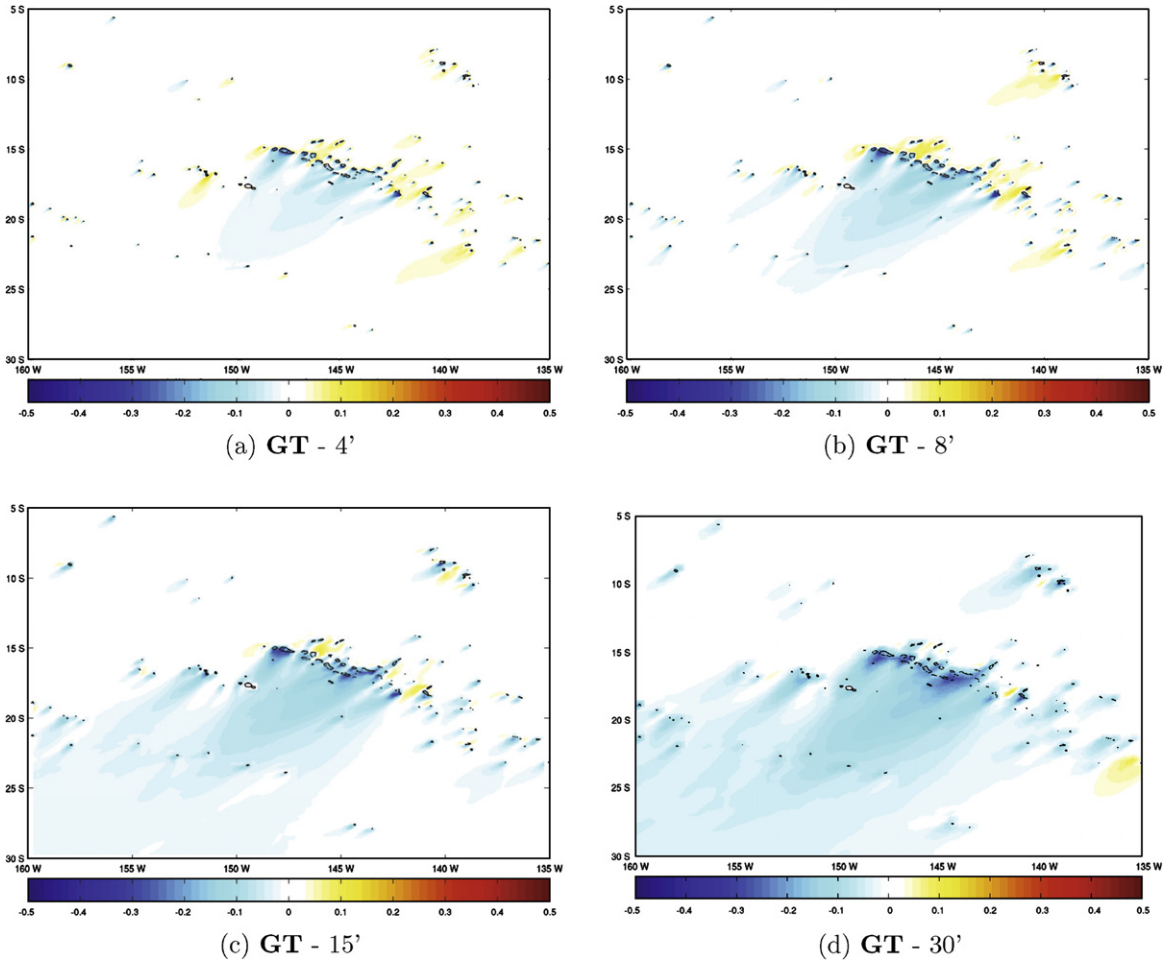

Fig. 12. Normalized difference plots (Ground Truth – Test Case) of wave heights for tests accounting for obstruction without including neighboring cell information (**OB-0**): (a) **GT-4′**; (b) **GT-8′**; (c) **GT-15′**; (d) **GT-30′**.

obstruction algorithm has been developed to account for the far field effects (at least 2–3 grid cells away) of islands that cannot be resolved in the grid. For accurate swell conditions close to islands the most appropriate approach is to use high resolution grids that actually resolve the islands.

Appendix A. Alleviating Garden Sprinkler Effects

Due to the discretized representation of the ocean spectrum in spectral wave models, spatial spreading of the spectrum occurs along discrete bands leading to what is known as the "Garden Sprinkler Effect" (GSE). Since our test cases consist of a monochromatic wave component in frequency, GSE effects arise from the discretization of the directional spectrum only. To avoid GSE effects the resolution should be such that the spreading (after the swell has crossed through the domain) should not be larger than the mesh size Booij and Holthuijsen (1987). This leads to a limit on the directional resolution

$$\Delta\theta < 1/N,$$

where N is the distance across the grid in the number of meshes. For a given spectral resolution the greatest GSE effects will be observed in the grid with the finest resolution. For the test cases here, the 2′ grid is the finest grid with $N = 751$. This leads to a desired directional resolution of $\Delta\theta \approx 0.075°$, which is not practical.

There are two alternative methods available in **WW3** for alleviating GSE. The first is a method proposed by Booij and Holthuijsen (1987) and hereby referred to as BH87. They considered the wave action equation for spectral bands (as opposed to spectral components) and developed an alternative spatial propagation scheme with diffusion terms in the propagation equation to account for continuous dispersion of the spectrum. The diffusion coefficients in BH87 depend on the spectral resolution and the swell age, and are given by

$$D_{ss} = \Delta c_g^2 T_s/12; \quad D_{nn} = c_g^2 \Delta\theta^2 T_s/12 \tag{A.1}$$

where, D_{ss}, D_{nn} are the diffusion coefficients along the direction of propagation and normal to the direction of propagation respectively, $\Delta c_g, \Delta\theta$ depend on the spectral resolution and T_s is a physical swell age. Though BH87 is

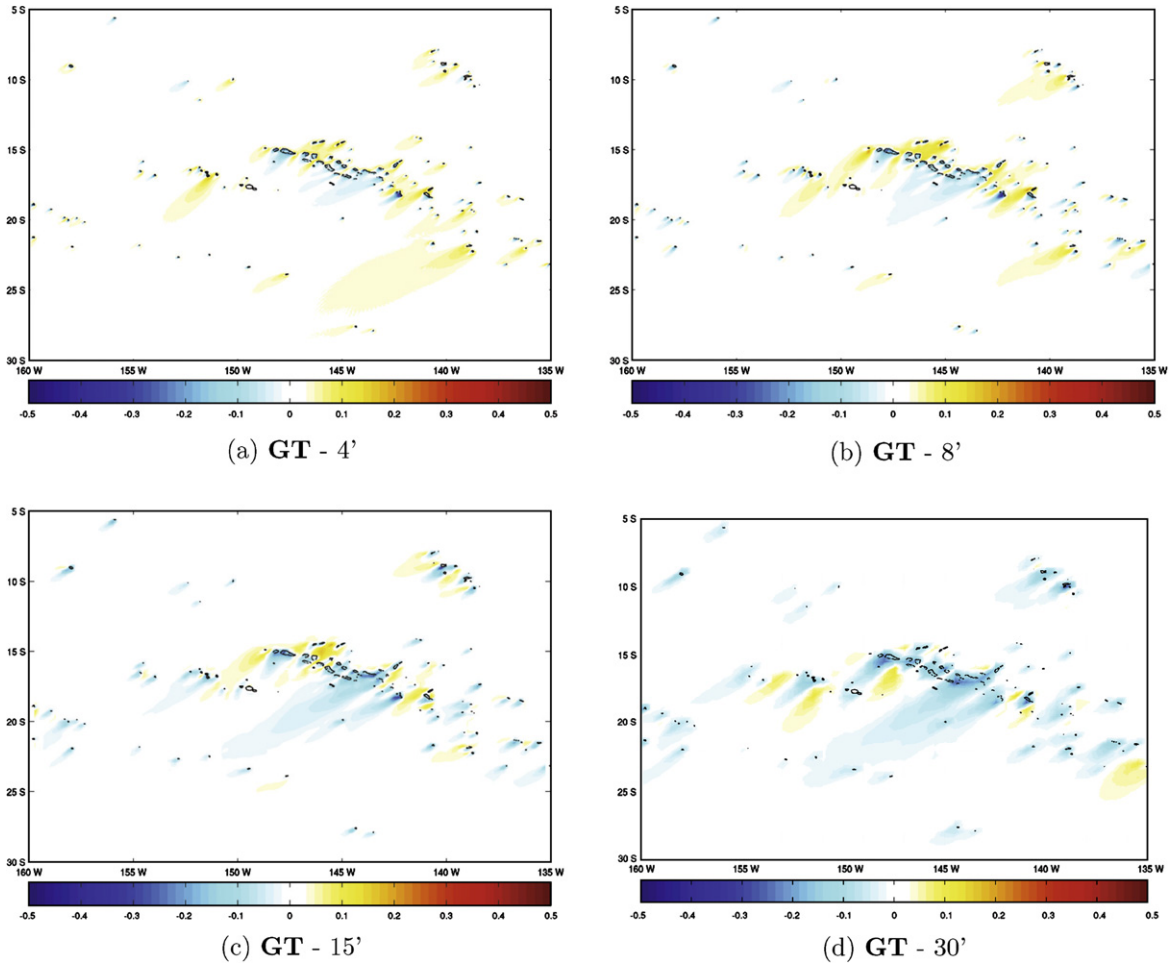

Fig. 13. Normalized difference plots (Ground Truth – Test Case) of wave heights for tests accounting for obstruction including information from neighboring cells to the right (for x) and up (for y) (**OB-1**): (a) **GT-4′**; (b) **GT-8′**; (c) **GT-15′**; (d) **GT-30′**.

adept at alleviating GSE, numerical stability requirements of this scheme puts a limit on the size of Δt for higher resolution grids (Tolman, 2002a.)

The second approach suggested by Tolman (2002a) (hereby referred to as T02) involves applying a local average (Fig. A.1). T02 uses a '9 point' stencil denoted by the solid circles in Fig. A.1 and linear interpolation to determine the wave heights at the shaded circles in Fig. A.1. The wave heights are then interpolated to the edges of the averaging box, which are then averaged with the wave height at the proper grid point. The dimensions of the averaging domain along the direction of propagation ($\vec{s}$) and normal to the direction of propagation ($\vec{n}$) are given by

$$\pm\gamma_{a,s}\Delta c_g\Delta t\vec{s}; \quad \pm\gamma_{a,n}c_g\Delta\theta\Delta t\vec{n} \tag{A.2}$$

where, Δc_g, $\Delta\theta$ correspond to the spectral resolution as in (A.1), Δt is the computational time step and $\gamma_{a,s}$, $\gamma_{a,n}$ are tuning parameters. Tolman (2002a) has shown that with the appropriate tuning parameters T02 gives virtually identical results as BH87 but without the additional computational cost of reduced time steps. Its computational efficiency makes T02 our preferred method of GSE alleviation. The disadvantage of this approach is that the averaging domain is time step dependent, which implies that if the tuning factors are left unchanged then the effectiveness of GSE alleviation decrease with increasing grid resolution. Ideally, we would like to have the alleviation to be determined by the spectral resolution and the swell age just like in BH87 and not be grid dependent. To do that we compare the two approaches and thus develop guidelines for the tuning parameters which would lead to the same level of GSE alleviation in all the grids, irrespective of their resolution.

For simplicity let us assume that the propagation direction is along one of the axes, namely the x axis. The interpolation and averaging approach of T02 then yields

$$\begin{aligned} F^{\star}_{i,j} = F_{i,j} &+ \frac{\beta_1}{\Delta t}6\Delta x[F_{i+1,j+1} - 2F_{i,j+1} + F_{i-1,j+1}] \\ &+ \frac{\beta_1}{\Delta t}6\Delta x[F_{i+1,j-1} - 2F_{i,j-1} + F_{i-1,j-1}] \\ &+ \frac{\beta_2}{\Delta t}6\Delta y[F_{i,j+1} - 2F_{i,j} + F_{i,j-1}] \end{aligned} \tag{A.3}$$

where $F_{i,j}$ correspond to the spectral estimate at the ith and jth node, $F^{\star}_{i,j}$ is the new average value and

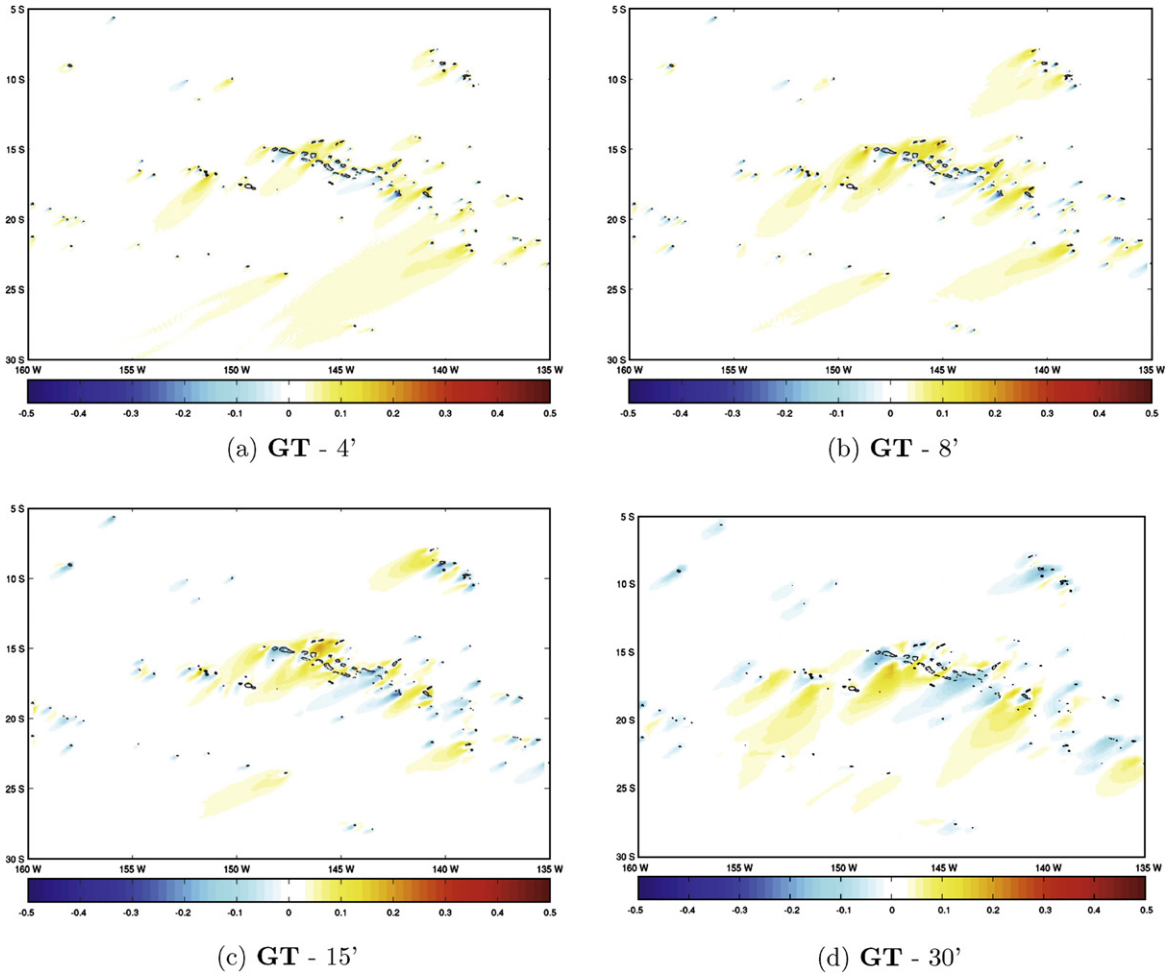

Fig. 14. Normalized difference plots (Ground Truth – Test Case) of wave heights for tests accounting for obstruction including information from neighboring cells in both directions (**OB-2**): (a) **GT-4′**; (b) **GT-8′**; (c) **GT-15′**; (d) **GT-30′**.

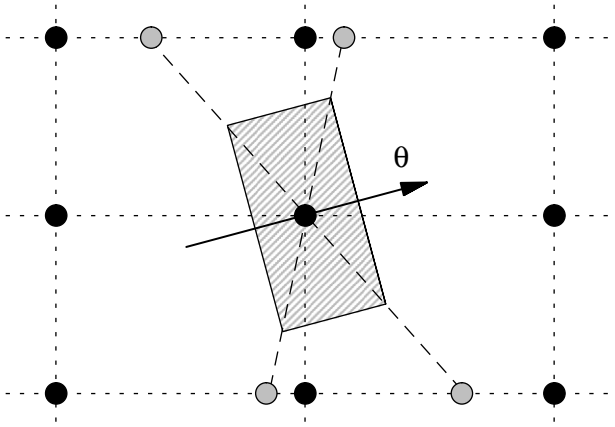

Fig. A.1. Averaging area for GSE alleviation in T02 (taken from Tolman, 2003).

$$\beta_1 \equiv \gamma_{a,s}\Delta c_g; \quad \beta_2 \equiv \gamma_{a,n} c_g \Delta\theta$$

Using Taylor series expansion and ignoring terms of the $O(\Delta t^2, \Delta x^3)$ we get

Table A.1
Tuning factors $(\gamma_{a,s}, \gamma_{a,n})$ used in **WW3** for alleviating GSE

Grid resolution	Tuning factor
2′	16
4′	8
8′	4
15′	2
30′	1

$$\frac{\partial F}{\partial t} = \frac{\beta_1 \Delta x}{3}\frac{\partial^2 F}{\partial x^2} + \frac{\beta_2 \Delta y}{3}\frac{\partial^2 F}{\partial y^2} \tag{A.4}$$

which is similar to the diffusion form of BH87. Comparing the diffusion coefficients in (A.4) and (A.1) yields

$$\gamma_{a,s} = \frac{\Delta c_g T_s}{4\Delta x}; \quad \gamma_{a,n} = \frac{\Delta\theta c_g T_s}{4\Delta y} \tag{A.5}$$

Eq. (A.5) provides a guide for setting the tuning factors to alleviate GSE based on swell age, grid and spectral resolution. It also indirectly helps determine the appropriate spectral resolution. Since T02 has been limited to a '9 point

stencil', the spectral resolution has to be fine enough that the averaging domain defined by (A.2) does not exceed the 9 point stencil. Which implies

$$\gamma_{a,s}\Delta c_g\Delta t < \Delta x; \quad \gamma_{a,n}c_g\Delta\theta\Delta t < \Delta y \tag{A.6}$$

Eqs. (A.5) and (A.6) have been obtained by assuming that the direction of propagation was along the x axis. In reality, the direction of propagation can change and in a grid with different dimensions along the two axes, the equations would be given by

$$\gamma_{a,s} = \frac{\Delta c_g T_s}{4\min(\Delta x, \Delta y)}; \quad \gamma_{a,n} = \frac{\Delta\theta c_g T_s}{4\min(\Delta x, \Delta y)} \tag{A.7}$$

$$\gamma_{a,s}\Delta c_g\Delta t < \min(\Delta x, \Delta y); \quad \gamma_{a,n}c_g\Delta\theta\Delta t < \min(\Delta x, \Delta y) \tag{A.8}$$

Eqs. (A.7) and (A.8) together determine the spectral resolution and tuning factors needed for T02 to effectively alleviate GSE.

For this experiment, the swell age T_s in Eqs. (A.7) and (A.8) has been set as 4 days (since that is the time needed for the swell to propagate through the grid). For the 2′ grid the spectral resolution was then limited by (A.8) and yielded

$$\Delta\theta < 5.38^\circ$$

Thus, the directional spectrum was discretized into 72 bins ($\Delta\theta = 5^\circ$). The corresponding tuning factors $(\gamma_{a,n}, \gamma_{a,s})$ required for the five different grids are given in Table A.1. This ensured that the results were not affected by GSE.

References

Booij, N., Holthuijsen, L.H., 1987. Propagation of ocean waves in discrete spectral wave models. Journal of Computational Physics, 307–326.

Chawla, A., Tolman, H.L., 2007. Automated grid generation for WAVEWATCH III. Technical Bulletin 254, NCEP/NOAA/NWS, National Center for Environmental Prediction, Washington, DC (April).

Hardy, T.A., Mason, L.B., McConochie, J.D., 2001. A wave model for the Great Barrier Reef. Ocean Engineering 28, 45–70.

Hardy, T.A., Young, I.R., 1996. Field study of wave attenuation on an offshore coral reef. Journal of Geophysical Research 101, 14311–14326.

Holthuijsen, L.H., Booij, N., Ris, R.C., Haagsma, I.G., Kieftenburg, A.T.M.M., Kriezi, E.E., 2001. SWAN Cycle III Version 40.11 User Manual. Delft University of Technology, Department of Civil Engineering, P.O. Box 5048, 2600 GA Delft, The Netherlands. Available from: <http://swan.ct.tudelft.nl>.

NGDC, 2006. 2-minute gridded global relief data (ETOPO2). Available from: <http://www.ngdc.noaa.gov/mgg/fliers/01mgg04.html>.

Tolman, H.L., 2002a. Alleviating the Garden Sprinkler Effect in wind wave models. Ocean Modelling 4, 269–289.

Tolman, H.L., 2002b. User manual and system documentation of WAVEWATCH III version 2.22. Technical Note 222, NCEP/NOAA/NWS, National Center for Environmental Prediction, Washington, DC (September).

Tolman, H.L., 2003. Treatment of unresolved islands and ice in wind wave models. Ocean Modelling 5, 219–231.

Tolman, H.L., 2006. Toward the third release of WAVEWATCH III: A multi-grid model version. JCOMM Techn. Rep. 34, WMO/TD – No. 1368, paper L1.

Wessel, P., Smith, W., 1996. A global self-consistent hierarchical high-resolution shoreline database. Journal of Geophysical Research 101 (B4), 8741–8743.